Dual-Active-Bridge Converter with Triple Phase Shift Control for a Wide Operating Voltage Range

[1]Yi-Hsuan Chen [1]Ta-Wei Huang [1]Shih-Hao Kuo [1]Yu-Chen Chang [1]Huang-Jen Chiu
[2] Serafin Bachman [2]Marek Jasiński

[1]Department of Electronics and Computer Engineering
National Taiwan University of Science and Technology
Taipei 106, Taiwan
*hjchiu@mail.ntust.edu.tw

[2]Institute of Control and Industrial Electronics
Warsaw University of Technology
00-662 Warszawa, Poland
*marek.jasinski@pw.edu.pl

***Abstract*—An optimal modulation scheme with Triple-Phase-Shift (TPS) control that increase efficiency in the whole load range is presented for a Dual Active Bridge (DAB) converter under wide output voltage range conditions. This paper provides a comprehensive analysis of the DAB with TPS modulation, identifying all the switching modes to operate the DAB where expressions for the transfer functions, the peak inductor current and RMS inductor current are provided. An analysis of minimum Peak Current and minimum RMS Current Control also are investigated. On this basic all-ZVS modulation scheme is originally proposed to improve light-load efficiency and to reduce the switching losses. A 15 kW prototype circuit is applied, and experimental results are presented to validate that the modulation and efficiency improvement are realized by applying the optimized modulation scheme. The experimental results also verify the effectiveness of the closed-loop control strategy.**

Index Terms*—Dual Active Bridge converter, Triple Phase Shift modulation, soft switching.

I. INTRODUCTION

Today, most microgrids include a large number of DC converter units, such as photovoltaic panels, energy storage systems, and electric vehicles, all of which require DC-DC converters for energy conversion. In some practical applications, converters with a wide range of voltage conversion ratios and bidirectional power flow control will be required; therefore, to comply with the current trend of environmental protection and high efficiency, it is particularly important to use a suitable converter architecture, modulation and control method [1]. Dual-Active-Bridge (DAB) converters rely on bidirectional power flow control, electrical isolation, high efficiency and high power density, and are now widely used in battery energy storage systems, solar photovoltaic panels [2]. The Single-Phase-Shift (SPS) control method is the most common and widely used control method of DAB at present because of its simplicity. However, in applications with a wide range of voltage conversion ratios, it may no longer have the advantages of zero-voltage switching conditions, and the RMS current, peak current and circulating current will increase significantly, resulting in a decrease in efficiency [3]. Therefore, this paper will adopt the Triple-Phase-Shift (TPS) control method for DAB converters applied to a wide range of output and is based on the algorithm for optimizing efficiency, including the operation principle of the control, the mathematical calculation of the algorithm, and the design process. We will conduct a detailed analysis and compare with SPS control, and finally will be verified with a 15 kW DAB converter platform.

II. DUAL-ACTIVE-BRIDGE CONVERTER

The DAB converter topology is shown in Figure 1. This topology has the advantages of circuit symmetry, bidirectional power flow, high power density, high efficiency, zero voltage switching, the output voltage can be increased or stepped down, and electrical isolation. In the ideal switching case where the duty cycle of the primary and secondary side switches is 50%, AC square waves with two voltage levels will be generated on both sides of the inductor. By controlling the phase shift angle, phase relationship and amplitude between the voltages on both sides of the inductor, And then control the direction and value of the power flow.

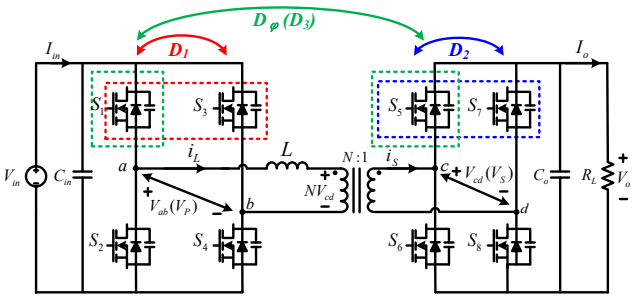

Fig.1 DC-DC Dual-Active-Bridge (DAB) Converter

In order to analyse, the following points are defined and assumed:

1. The duty cycle of all switches is 50%, the upper and lower arm switches are complementary, and dead time is ignored.

2. Ignore the influence of the parasitic capacitance Coss of each switch and the magnetizing inductance.

3. The definitions of the phase shift angles D1, D2, D3 and Dφ between the power switches are shown in Figure 2. The relationship between D3 and Dφ is defined as for formula (1), and the defined phase shift angles are all phase shift angles and half period π.

4. The inductance L in Figure 1 is defined as the sum of the transformer leakage inductance L_{lk} and the external series inductance L_{pri}, the transformer turns ratio is N, and the voltage conversion ratio M is defined as equation (2).

$$D_3 = D_\varphi + \frac{D_1}{2} - \frac{D_2}{2} \tag{1}$$

$$M = \frac{NV_o}{V_{in}} \tag{2}$$

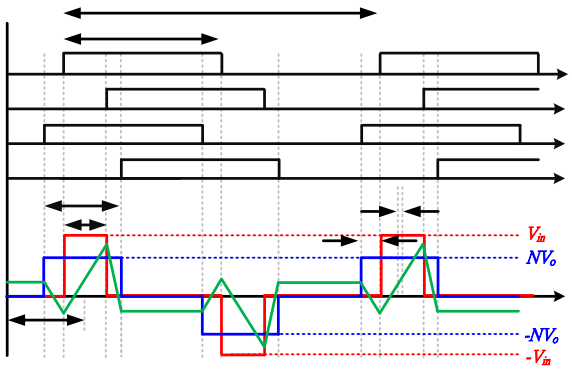

Fig.2 The relationship between phase shift and the switching signals.

III. TRIPLE-PHASE-SHIFT MODULATION

This section will distinguish and define all operating modes of the TPS control method according to different phase shift angles, and discuss the circuit characteristics, including the operation principle, power function derivation, peak current and RMS current analysis, and zero voltage condition calculation. The minimum peak value control method with a mathematical algorithm, and propose a new modulation method—full range zero-voltage control method to improve the defect that the minimum peak value control method cannot achieve zero voltage switching in the light load range. At the same time, define the time point of the positive edge of V_p as t_{1LH}, the negative edge as t_{1HL}. The positive edge of V_s as t_{2LH}, and the negative edge as t_{2HL}. Taking the definition of the relationship between the phase shift angle and the switching signal in Figure 2 as the derivation basis, the time points of the positive and negative edges of the primary and secondary sides of the transformer can be expressed in terms of the phase shift angle relation, and the result is shown in equation (3).

$$\begin{aligned} t_{1LH} &= \frac{T_s}{2}(\frac{1}{2}-\frac{D_1}{2}) \\ t_{1HL} &= \frac{T_s}{2}(\frac{1}{2}+\frac{D_1}{2}) \\ t_{2LH} &= \frac{T_s}{2}(D_\varphi+\frac{1-D_2}{2}) \\ t_{2HL} &= \frac{T_s}{2}(D_\varphi+\frac{1+D_2}{2}) \end{aligned} \tag{3}$$

Due to the symmetry characteristics of the DAB circuit, the positive power flow and the negative power flow have the same analysis results [4], so if only the positive power flow is considered, and the inductor current waveform is based on the transformer turns ratio N, inductance Differentiate analysis and define the modes based on the quantity L, switching frequency fs, the input voltage Vin, output voltage Vo, and phase shift angle parameters $D1$, $D2$, $D\varphi$. There are four possible combinations for TPS: Case1, Case2, Case3, Case4, As shown in Table 1.

Table.1 Definition of TPS control combination

Case i	Definition
1	$Vin \geq NVo$, $D1>D2$
2	$Vin \geq NVo$, $D1 \leq D2$
3	$Vin<NVo$, $D1>D2$
4	$Vin<NVo$, $D1 \leq D2$

According to the different operating ranges of Dφ in 1≥Dφ>0, seven modes are subdivided under various combinations, namely: SM1, SM2, SM2*, SM3, SM3*, SM4, SM5, When the negative power flow is added, there will be 56 operating conditions under the TPS control method of the DAB circuit. Due to the symmetrical characteristics of the DAB circuit, it can be seen that under positive power flow, Case1 and Case4 are defined as the relationship between the inductance primary and secondary side cross-voltage (Vin, NVo) mutual adjustment, so the power function and the current result of function deduction will be the same, and Case2 will be the same as Case3 analysis [5]. Therefore, the following is to help simplify the analysis, and will only discuss and study of Case1 and Case2. Table 2 lists the seven mode definitions of Case1 and Case2.

Table.2 Definition of $D\varphi$ range for each mode of Case1 and Case2:

SMi	Case1	Case2
SM1	$0<D_\varphi \leq (\frac{D_1-D_2}{2})$	$0<D_\varphi \leq (\frac{D_2-D_1}{2})$
SM2	$(\frac{D_1-D_2}{2})<D_\varphi \leq (\frac{D_1+D_2}{2})$	$(\frac{D_2-D_1}{2})<D_\varphi \leq (\frac{D_2+D_1}{2})$
SM2*	$(\frac{D_1-D_2}{2})<D_\varphi \leq (1-\frac{D_1+D_2}{2})$	$(\frac{D_2-D_1}{2})<D_\varphi \leq (1-\frac{D_2+D_1}{2})$
SM3	$(\frac{D_1+D_2}{2})<D_\varphi \leq (1-\frac{D_1+D_2}{2})$	$(\frac{D_2+D_1}{2})<D_\varphi \leq (1-\frac{D_2+D_1}{2})$
SM3*	$(1-\frac{D_1+D_2}{2})<D_\varphi \leq (\frac{D_1+D_2}{2})$	$(1-\frac{D_2+D_1}{2})<D_\varphi \leq (\frac{D_2+D_1}{2})$
SM4	$(1-\frac{D_1+D_2}{2})<D_\varphi \leq (1-\frac{D_1-D_2}{2})$	$(1-\frac{D_2+D_1}{2})<D_\varphi \leq (1-\frac{D_2-D_1}{2})$
SM5	$(1-\frac{D_1-D_2}{2})<D_\varphi \leq 1$	$(1-\frac{D_2-D_1}{2})<D_\varphi \leq 1$

List the transfer functions of Case1 and Case2, and use the SM1 mode of Case2 as a benchmark to derive the mathematical equation of the transmission power Po. Consider the characteristic that the inductor current is symmetric during the switching period, and the derivation will only be made for half of the switching period. Its definition is as formula (4). It can be seen from the action state in Figure 6 that the inductor primary side voltage Vp is the input voltage Vin only from $t2$ to $t4$ during half of the cycle, and $t0$ to $t2$ and $t4$ to $t7$ are all zero voltages, so only the power from $t2$ to $t4$ is required. Calculated as equation (5), and the output power function can be obtained as equation (6).

$$P_o = \frac{1}{T_s/2}\int_0^{T_s/2} V_P(t)\times I_L(t)dt = \frac{1}{T_s/2}\int_0^{T_s/2} V_S(t)\times I_S(t)dt \tag{4}$$

$$P_o = \frac{1}{T_s/2}\int_{t_2}^{t_4} V_P(t)\times I_L(t)dt \tag{5}$$

$$P_o = \frac{V_{in}NV_oD_1D_\varphi}{2Lf_s} \tag{6}$$

The derivation process and steps of the different modes are similar. The transfer functions of Case1 and Case2 are listed in Table 3. The relationship between the per-unit value (pu) and the phase shift angle of Case1 and Case2 is shown in Table 3. the current of Case1 and Case2 are shown in Table 4.

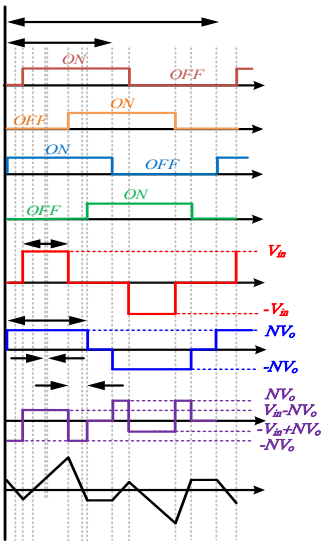

Fig.6 Action state diagram of SM1 mode of Case2

Table.3 Triple Phase Shift (TPS) control Case1 and Case2 output power function in each mode

SMi	*Case1*	*Case2*
SM1	$\frac{V_{in}NV_oD_2D_\varphi}{2Lf_s}$	$\frac{V_{in}NV_oD_1D_\varphi}{2Lf_s}$
SM2 *SM2**	$\frac{V_{in}NV_o}{4Lf_s}\left[D_\varphi(D_1+D_2-D_\varphi)-\frac{(D_1-D_2)^2}{4}\right]$	
SM3	$\frac{V_{in}NV_oD_1D_2}{4Lf_s}$	
*SM3**	$\frac{V_{in}NV_o}{2Lf_s}\left[D_\varphi(1-D_\varphi)-\frac{(D_1-1)^2+(D_2-1)^2}{4}\right]$	
SM4	$\frac{V_{in}NV_o}{4Lf_s}\left[(1-D_\varphi)(D_1+D_2+D_\varphi-1)-\frac{(D_1-D_2)^2}{4}\right]$	
SM5	$\frac{V_{in}NV_oD_2(1-D_\varphi)}{2Lf_s}$	$\frac{V_{in}NV_oD_1(1-D_\varphi)}{2Lf_s}$

Table.4 The current formula of each mode of the TPS control Case1 and Case2

SMi	*Case1*	*Case2*
SM1	$i_L(t_{1LH})=-i_L(t_{1HL})=-\frac{D_1V_{in}-D_2NV_o}{4Lf_s}$ $i_L(t_{2LH})=-\frac{D_2V_{in}-2V_{in}D_\varphi-D_2NV_o}{4Lf_s}$ $i_L(t_{2HL})=\frac{D_2V_{in}+2V_{in}D_\varphi-D2NV_o}{4Lf_s}$	$i_L(t_{1LH})=-\frac{D_1V_{in}-2D_\varphi NV_o-D_1NV_o}{4Lf_s}$ $i_L(t_{1HL})=\frac{D_1V_{in}+2NV_oD_\varphi-D_1NV_o}{4Lf_s}$ $i_L(t_{2HL})=-i_L(t_{2LH})=\frac{D_1V_{in}-D_2NV_o}{4Lf_s}$
SM2	$i_L(t_{1LH})=-i_L(t_{2HL})=-\frac{D_1V_{in}-D_2NV_o}{4Lf_s}$	
*SM2**	$i_L(t_{1HL})=\frac{D_1V_{in}+2NV_oD_\varphi-D_2NV_o}{4Lf_s}$ $i_L(t_{2LH})=-\frac{D_2V_{in}-2V_{in}D_\varphi-D_2NV_o}{4Lf_s}$	
SM3	$i_L(t_{1LH})=-i_L(t_{2HL})=-\frac{D_1V_{in}-D_2NV_o}{4Lf_s}$ $i_L(t_{1HL})=-i_L(t_{2LH})=\frac{D_1V_{in}+D_2NV_o}{4Lf_s}$	
*SM3**	$i_L(t_{1LH})=-\frac{D_1V_{in}+D_1NV_o-2NV_o(1-D_\varphi)}{4Lf_s}$ $i_L(t_{1HL})=\frac{D_1V_{in}-D_1NV_o+2NV_oD_\varphi}{4Lf_s}$ $i_L(t_{2LH})=-\frac{D_2V_{in}-D_2NV_o-2V_{in}D_\varphi}{4Lf_s}$ $i_L(t_{2HL}-\frac{T_s}{2})=\frac{D_2V_{in}+D_2NV_o-2V_{in}(1-D_\varphi)}{4Lf_s}$	
SM4	$i_L(t_{1LH})=-\frac{D_1V_{in}+D_1NV_o-2NV_o(1-D_\varphi)}{4Lf_s}$ $i_L(t_{1HL})=i_L(t_{2LH})=\frac{D_1V_{in}-D_1NV_o+2NV_oD_\varphi}{4Lf_s}$ $i_L(t_{2HL}-\frac{T_s}{2})=\frac{D_2V_{in}+D_2NV_o-2V_{in}(1-D_\varphi)}{4Lf_s}$	
SM5	$\frac{V_{in}NV_oD_2(1-D_\varphi)}{2Lf_s}$	$\frac{V_{in}NV_oD_1(1-D_\varphi)}{2Lf_s}$

The inductor current i_L will affect the switching loss and conduction loss of the circuit, so this section will analyze the RMS current and peak current of the inductor for each mode of the TPS control, Case1 and Case2. Due to the symmetry of the inductor current i_L, the effective value current is calculated with half the switching period *Ts/2*, as shown in equation (7).

$$I_{L(RMS)}=\sqrt{\frac{1}{T_s/2}\int_0^{T_s/2}i_L(t)^2dt} \tag{7}$$

Figures 7 respectively show the three-dimensional diagrams of the relationship between the effective value of the inductance of Case1 and Case2, the per-unit value (p.u) of the peak current and the phase shift angle. SM4 and SM5 modes in Case1 and Case2 have generally higher current values than other modes, so larger conduction losses will be caused under the same output power. The TPS control.

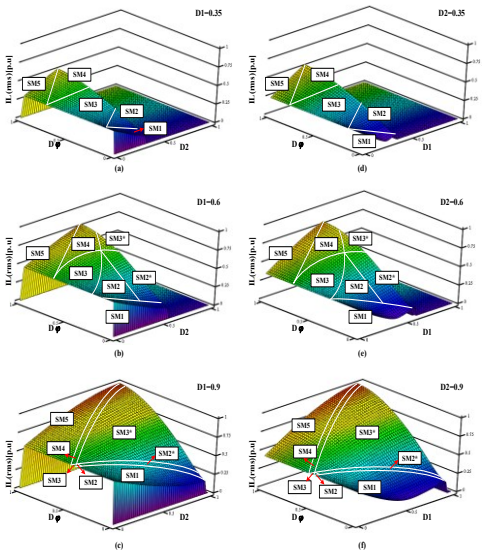

Fig.7 Three-dimensional diagrams of the RMS current and phase shift angle of the inductors in Case1 and Case2:

(a)*Case1, D1=0.35*、(b) *Case1, D1=0.6*、(c) *Case1, D1=0.9*、

(d) *Case2, D2=0.35*、(e) *Case2, D2=0.6*、(f) *Case2, D2=0.9*

In the TPS control, there will be a combination of multiple phase shift angles under the same output power, and the inductor current waveform will also be different in each mode. It will be necessary to calculate with mathematical tools to find the best phase shift angle parameter. First, analyze the current in each mode under Case1 and Case2, due to the relationship between

virtual power and various current characteristics, the circuit will not be considered to operate in SM4 and SM5 modes; from Table 3 and Table 4 we can see that Case1 and some modes of Case 2 have the same output power and point current value. The SM3 mode has a larger phase shift angle Dφ compared to the SM1 or SM2 mode. Therefore, the SM3 mode will not be considered; the SM1 mode of Case1 has a larger peak current than the SM1 mode of Case2, so the SM1 mode of Case1 will not be considered. In the end, the required analysis mode can be simplified as listed below:

- SM1 of Case2
- SM2 of Case1 and Case2 (the analysis of both is the same)
- SM3* of Case1 and Case2 (the analysis of both is the same)

In order to obtain the maximum phase shift angle combination (D1_opt, D2_opt, Dφ_opt) corresponding to the minimum peak current $I_{peak(min)}$ within the condition range of the specific mode, a mathematical tool is used here- Karush-Kuhn-Tucker Conditions, hereafter referred to as KKT conditions the general formula is as (8).

$$L(x,\lambda,\mu)=f(x)+\sum_{i=1}^{m}\lambda_i g_i(x)+\sum_{j=1}^{q}\mu_j h_j(x) \tag{8}$$

The minimum peak value, the minimum effective value and the best phase shift angle D_{1_opt}, D_{2_opt}, and D_{φ_opt} of the SM1 mode of Case2 in the output power Pon can be obtained as equation (9).

$$\begin{aligned} D_{1\_opt}&=\sqrt{\frac{2P_{on}}{(1-M)\pi}}\\ D_{2\_opt}&=\sqrt{\frac{2P_{on}}{M^2(1-M)\pi}}\\ D_{\varphi\_opt}&=\frac{\sqrt{2(1-M)\pi P_{on}}}{2\pi M} \end{aligned} \tag{9}$$

After summarizing the range of SM1 to SM3* and considering all the conditions of the voltage conversion ratio M, the optimized phase shift angles of the minimum peak current and the minimum effective value can be listed in all cases, as shown in Table 5.

Table.5 Optimized phase shift angle value of minimum peak value and RMS value current control modulation

M / Power range	M<1	M>1
$P\in[0,P_{o1}]$	$D_{1\_opt}=\sqrt{\frac{2P_{on}}{(1-M)\pi}}$ $D_{2\_opt}=\sqrt{\frac{2P_{on}}{M^2(1-M)\pi}}$ $D_{\varphi\_opt}=\frac{\sqrt{2(1-M)\pi P_{on}}}{2\pi M}$	$D_{1\_opt}=\frac{1}{M}\sqrt{\frac{2P_{on}}{M(M-1)\pi}}$ $D_{2\_opt}=\sqrt{\frac{2P_{on}}{M(M-1)\pi}}$ $D_{\varphi\_opt}=\sqrt{\frac{2P_{on}(M-1)}{M\pi}}$
$P\in[P_{o1},M\pi/4]$	$D_{1\_opt}=1-(1-M)\sqrt{\frac{M\pi-4P_{on}}{(1-2M+2M^2)M\pi}}$ $D_{2\_opt}=1-$ $D_{\varphi\_opt}=\frac{1}{2}-\frac{1}{2}\sqrt{\frac{M(M\pi-4P_{on})}{(1-2M+2M^2)\pi}}$	$D_{1\_opt}=1$ $D_{2\_opt}=1-\sqrt{(1-\frac{4P_{on}}{M\pi})\frac{(M-1)^2}{(M-1)^2+1}}$ $D_{\varphi\_opt}=1-\sqrt{2D_{2\_opt}-D_{2\_opt}^2-\frac{4P_{on}}{M\pi}}$

The minimum peak value and minimum effective value current control method is within the output power range of P∈[0,Po1], only two switches can achieve zero voltage switching. Therefore, the following will analyze the zero-voltage switching conditions and interval states considering the resonance energy in the minimum peak value and minimum effective value current control method in the P∈[0,Po1] interval, and propose a full-range zero-cut control method to improve the inability to zero-voltage switching The lack of this improves the overall efficiency of the circuit. By deriving the resonant energy of a switch dead zone, taking the SM1 mode of Case 2 as an example, the minimum voltage switching current can be obtained as shown in Table 6.

Table 6 Zero voltage switching conditions of SM1 of Case2

Switches	*Zero-voltage switching conditions*
S1	$i_{L(t2)}\le I_{\min\_s1}(-\sqrt{\frac{2V_{in}^2C_{oss}(1-2M)}{L}})$
S3	$i_{L(t4)}\ge I_{\min\_s3}(\sqrt{\frac{2V_{in}^2C_{oss}(1-2M)}{L}})$
S5	$i_{L(t0)}\ge I_{\min\_s5}(\sqrt{\frac{2V_o^2C_{oss}}{L}})$
S7	$i_{L(t6)}\le I_{\min\_s7}(-\sqrt{\frac{2V_o^2C_{oss}}{L}})$

The following will derive the optimal value of the phase shift angle of the full range zero-cut control method under the condition that the voltage conversion ratio is less than 1 (M<1). Control the value of the phase shift angle combination so that the current at the point of entering the dead zone is equal to the minimum current Imin required for zero-voltage switching. It can be seen from Table 4 that the output power function of the SM1 mode of Case2 is related to the phase shift angles D1 and Dφ. The zero-voltage switching achieved by the S1 switch will be related to the current at point $i_{L(t2)}$, and then it can be seen from Table 4 that the current remains unchanged in the specifications. In this case, it will be determined by the phase shift angle D1 and Dφ.

Conculsion

This article has aiming at Triple Phase Shift control with efficiency optimization control method to reduce the loss of the converter and improve the overall efficiency of the converter .

Reference

[1] B. Zhao, Q. Song, W. Liu and Y. Sun, “A Synthetic Discrete Design Methodology of High-Frequency Isolated Bidirectional DC/DC Converter for Grid-Connected Battery Energy Storage System Using Advanced Components,” in IEEE Transactions on Industrial Electronics, vol. 61, no. 10, Oct. 2014.

[2] L. Xue, Z. Shen, D. Boroyevich, P. Mattavelli and D. Diaz, “Dual Active Bridge-Based Battery Charger for Plug-in Hybrid Electric Vehicle With Charging Current Containing Low Frequency Ripple,” in IEEE Transactions on Power Electronics, vol. 30, no. 12, Dec. 2015.

[3] H. Bai, Z. Nie, and C.Mi, “Experimental comparison of traditional phaseshift, dual-phase-shift, and model-based control of isolated bidirectional dc-dc converters,” IEEE Trans. Power Electron., vol. 25, no. 6, pp. 1444–1449, Jun. 2010.

[4] X. Liu et al., “Novel Dual-Phase-Shift Control With Bidirectional Inner Phase Shifts for a Dual-Active-Bridge Converter Having Low Surge Current and Stable Power Control,” in IEEE Transactions on Power Electronics, vol. 32, no. 5, pp. 4095-4106, May 2017.

[5] Calderon, C., Barrado, A., Rodriguez, A., Alou, P., Lazaro, A., Fernandez, C. and Zumel, P. “General Analysis of Switching Modes in a Dual Active Bridge with Triple Phase Shift Modulation.”, Energies,2018.